`

Supplementary Materials for

Localised thermal levering events drive spontaneous kinetic oscillations in catalysis

Authors: Donato Decarolis[1,2], Monik Panchal[2,3], Matthew Quesne[1,2], Khaled Mohammed[4], Shaojun Xu[1,2], Mark Isaacs[3,5], Luke L. Keenan[6], Takuo Wakisaka[7], Kohei Kusada[7,8], Hiroshi Kitagawa[7], C. Richard A. Catlow[1,2,3], Emma K. Gibson[2,8], Alexandre Goguet[2,9*], Peter P. Wells[2,4,6*]

[1] Cardiff Catalysis Institute, School of Chemistry, Cardiff University, Cardiff CF10 3AT, UK

[2] UK Catalysis Hub, Research Complex at Harwell, Rutherford Appleton Lab, Harwell, Oxfordshire OX11 0FA, UK

[3] Department of Chemistry, University College London, 20 Gordon St., London WC1 HOAJ, UK

[4] School of Chemistry, University of Southampton, Southampton SO17 1BJ, United Kingdom

[5] Harwell XPS, Research Complex at Harwell, Rutherford Appleton Laboratory, Didcot OX11 0FA, UK

[6] Diamond Light Source, Harwell Science and Innovation Campus, Didcot OX11 0DE, Oxfordshire, United Kingdom

[7] Division of Chemistry, Graduate School of Science, Kyoto University, Kitashirakawa-Oiwakecho, Sakyo-ku, Kyoto, 606-8502, Japan

[8] The Hakubi Center for Advanced Research, Kyoto University, Kitashirakawa-Oiwakecho, Sakyo-ku, Kyoto, 606-8502, Japan

[9] School of Chemistry, Joseph Black Building, University of Glasgow, Glasgow G12 8QQ, United Kingdom

[10] Queen's University Belfast, School of Chemistry, David Keir Building, Stranmillis Rd, Belfast BT9 5AG, United Kingdom

*Corresponding authors: p.p.wells@soton.ac.uk, a.goguet@qub.ac.uk

`

Materials and Methods

Sample Characterisation

Transmission electron microscopy

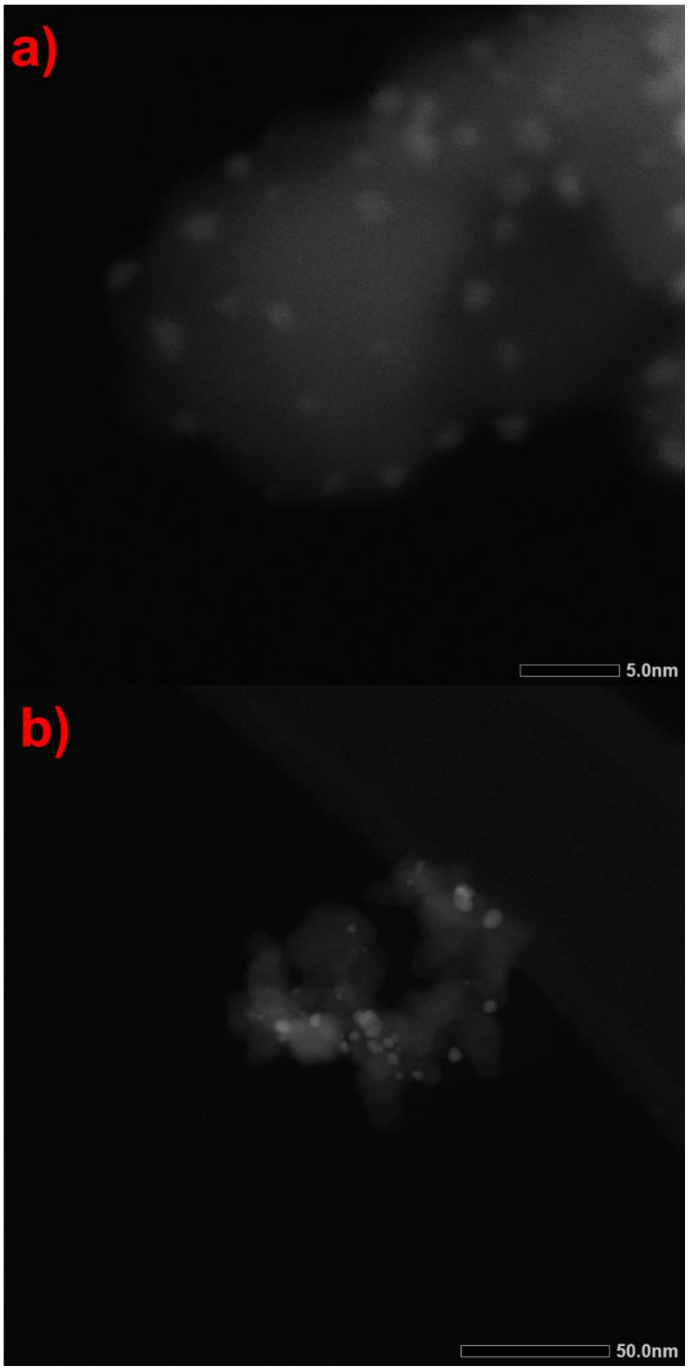

Figure S1. Representative STEM-HAADF image of the Rh/Al2O3 catalyst in (a) the unused state and (b) the used state.

`

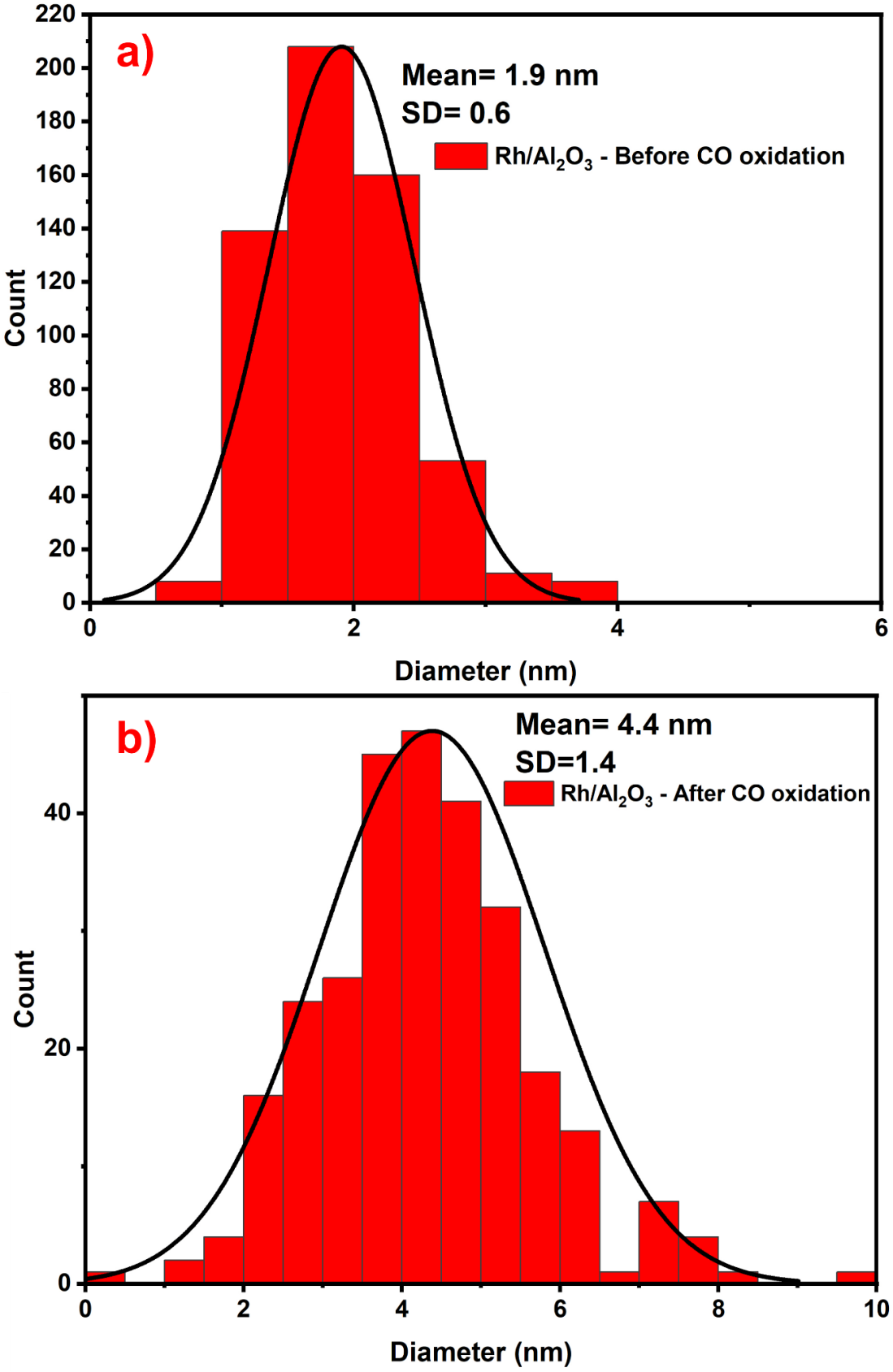

Figure S2. Particle size distribution for Rh/Al_2O_3 in (a) the unused state and (b) the used state

`

Combined *operando* EDE/DRIFTS measurement

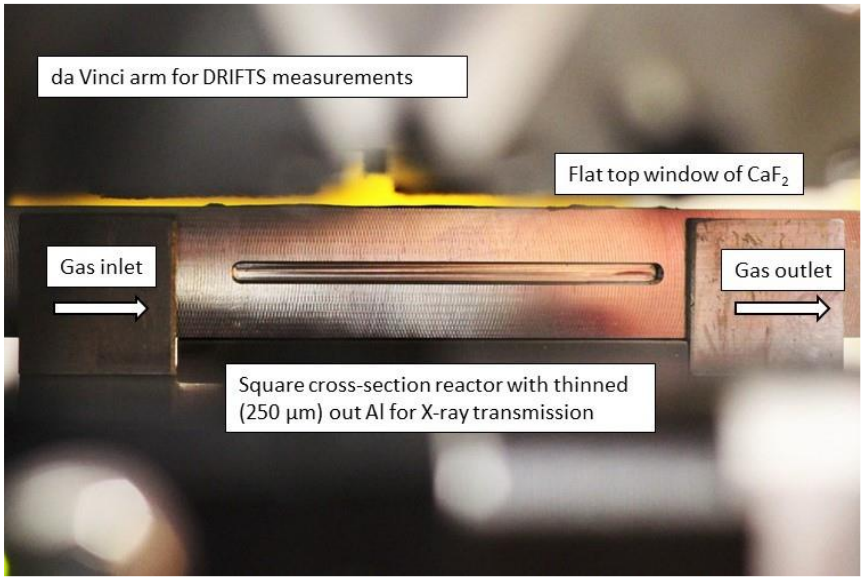

Figure S3. Photograph of the aluminium EDE/DRIFTS reaction cell

Supplementary Text

Radiation damage evaluation

In order to check for any radiation damage, we dosed the sample for a total of 30 min and checked the intensity of the first XANES peak (the “white-line”). As it can be seen in figure S2-4 these radiation damage could be significant and affect the result of the experiment.

`

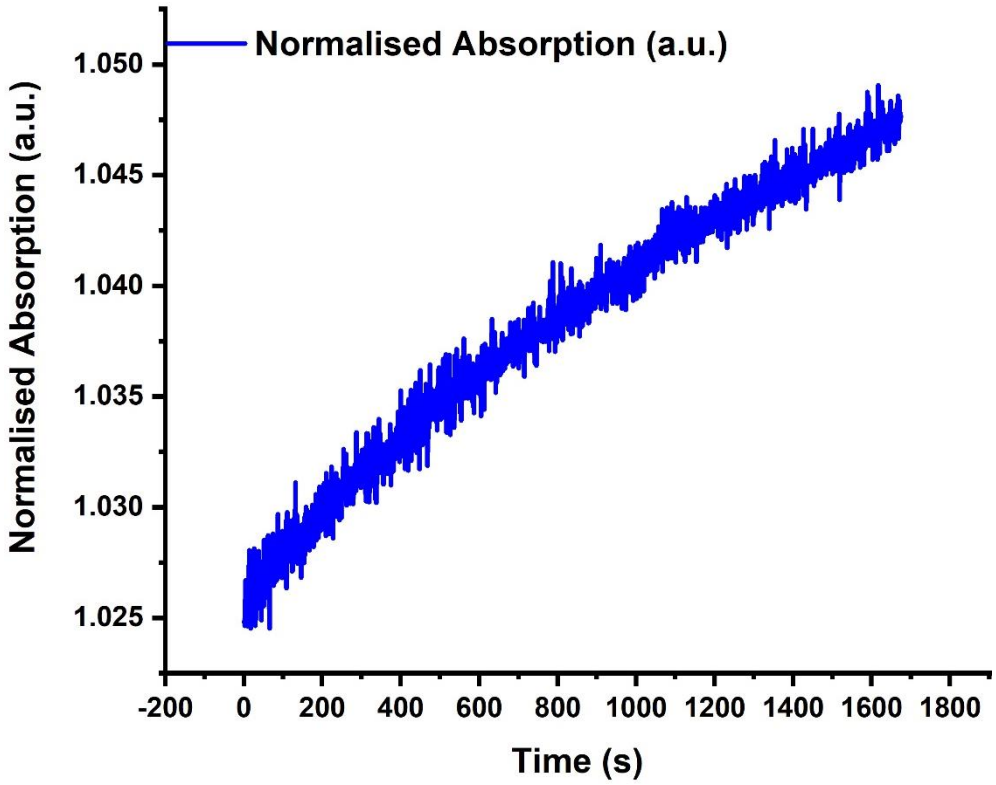

Figure S4. Rh-K edge XANES trace as function of time under Ar at room temperature before radiative damage prevention.

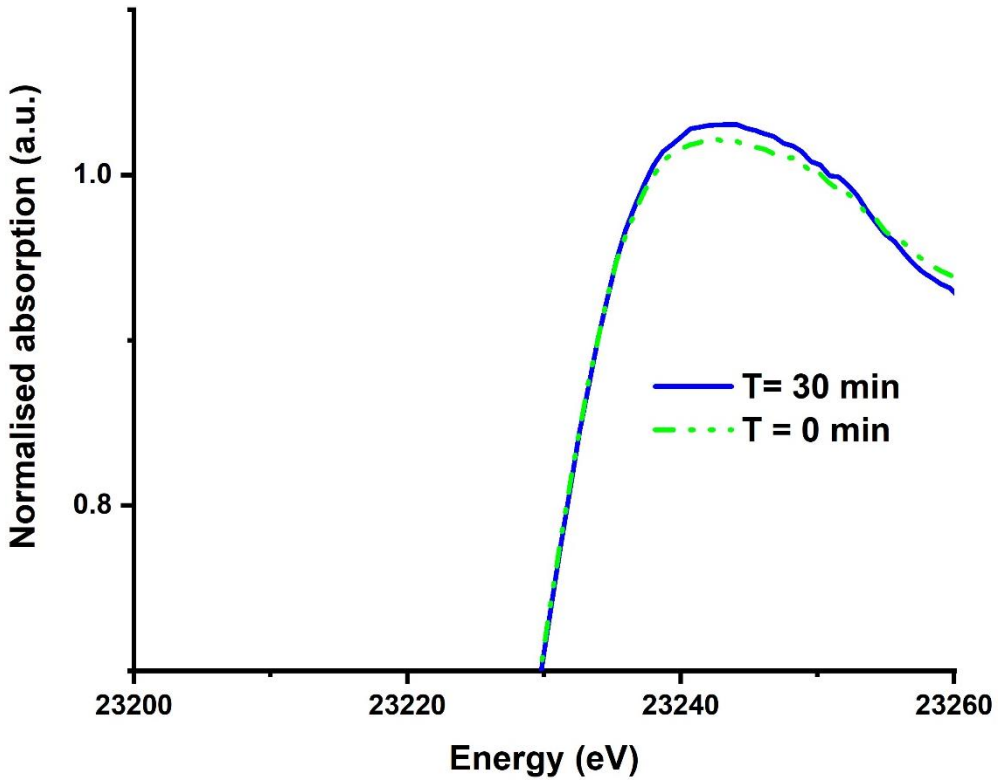

`

Figure S5. Rh-K edge XANES spectra under Ar at 0 and 30 min before radiative damage prevention

In order to reduce this effect, we have reduced the beam intensity by a factor of 9.7% and added Mo and Zn filter in order to further reduce the intensity and the subsequent beam damage, paired with a removal of all the water present in the system. This results in no change after the same procedure is applied again to check for radiative damage.

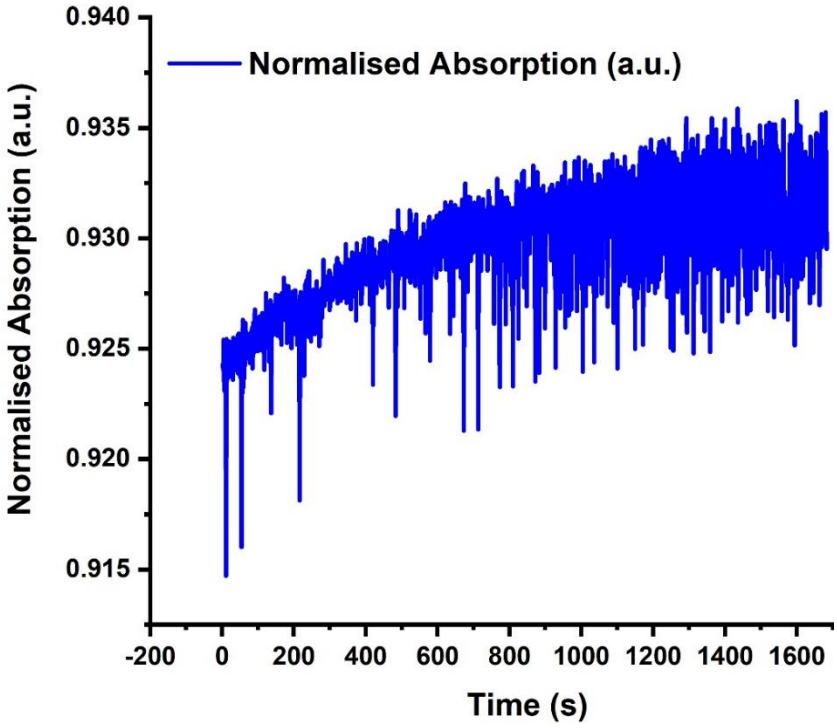

Figure S6. Rh-K edge XANES trace as function of time during under Ar at room temperature after radiative damage prevention.

`

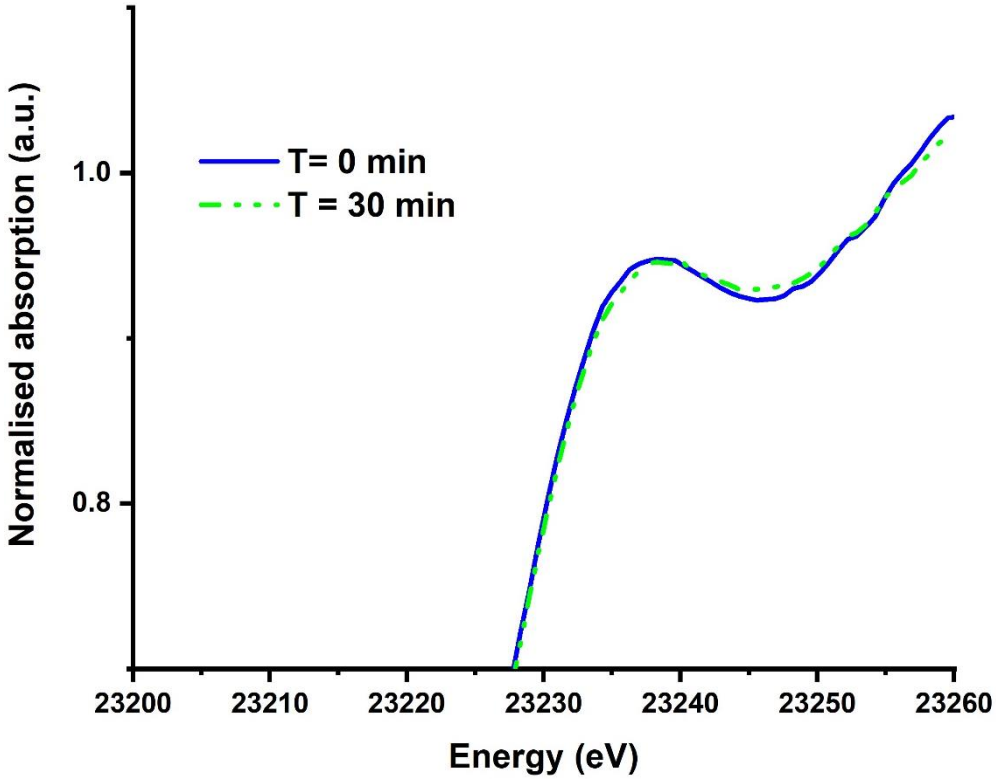

Figure S7. Rh-K edge XANES spectra under Ar at 0 and 30 min after radiative damage prevention

X-ray absorption spectroscopy results

`

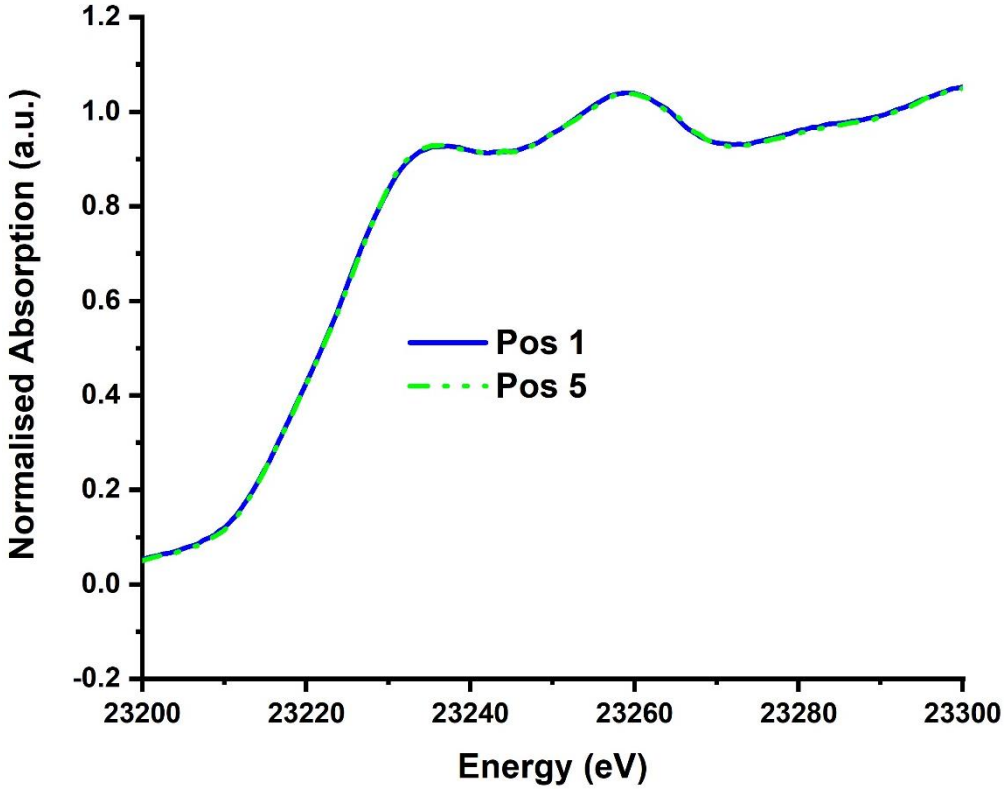

Figure S8 XANES of different position after cleaning cycle

`

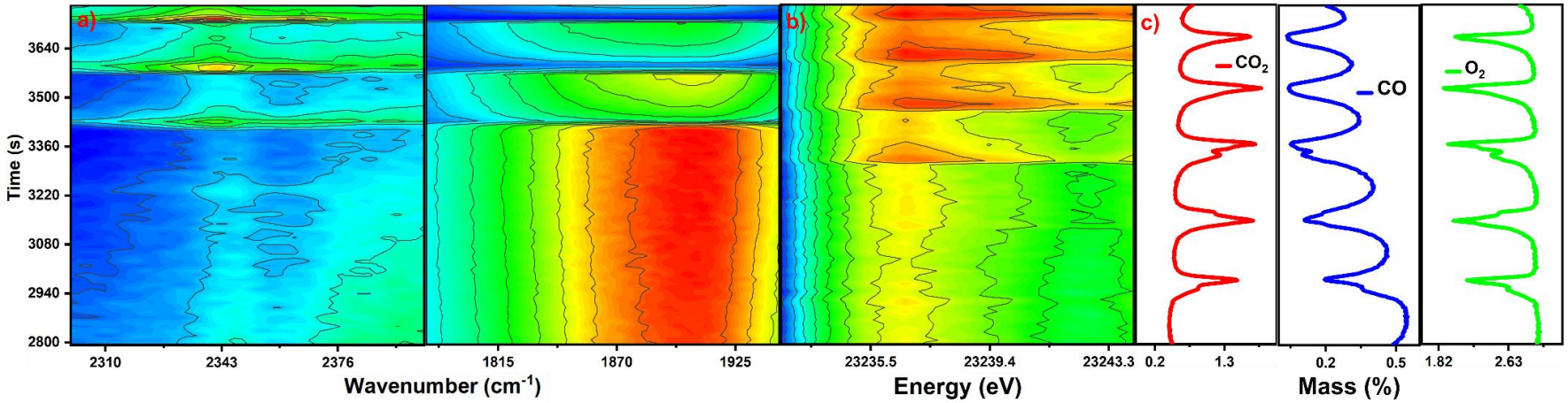

Figure S9 From left to right: a) DRIFTS signature for CO (left) and CO_2 (right) evolution; b) XANES evolution; c) evolution of CO_2, CO, and O_2 concentration as function of time for the position 1.

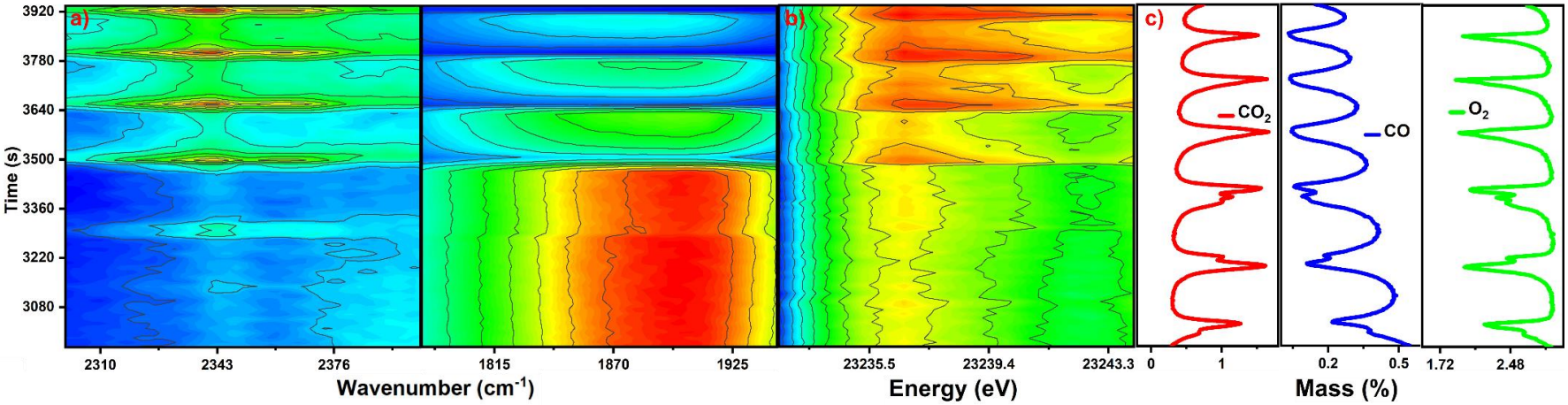

Figure S10 From left to right: a) DRIFTS signature for CO (left) and CO_2 (right) evolution; b) XANES evolution; c) evolution of CO_2, CO, and O_2 concentration as function of time for the position 2.

`

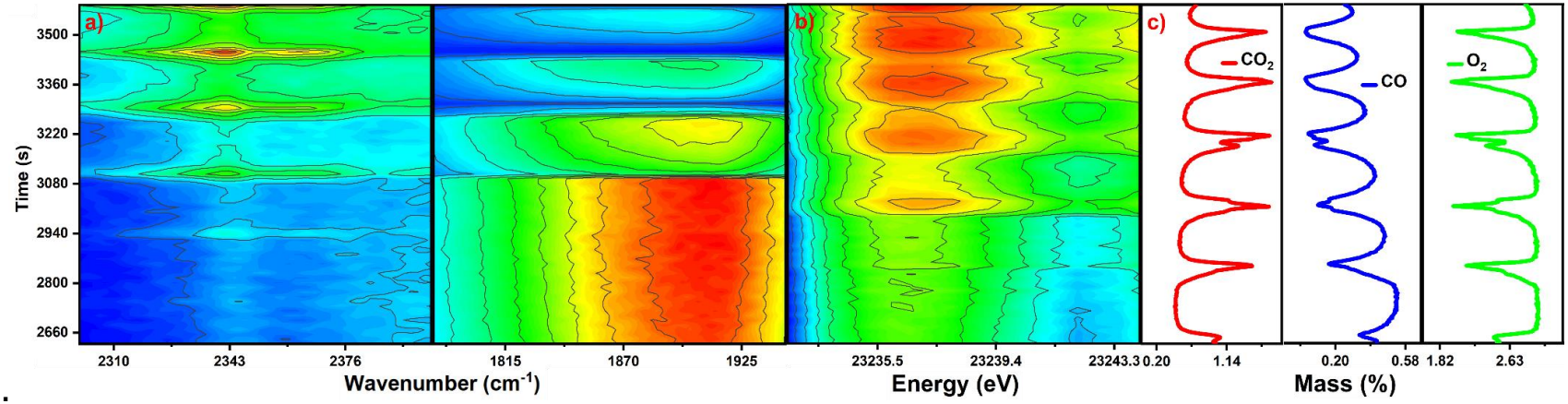

.

Figure S11 From left to right: a) DRIFTS signature for CO (left) and CO_2 (right) evolution; b) XANES evolution; c) evolution of CO_2, CO, and O_2 concentration as function of time for the position 3.

`

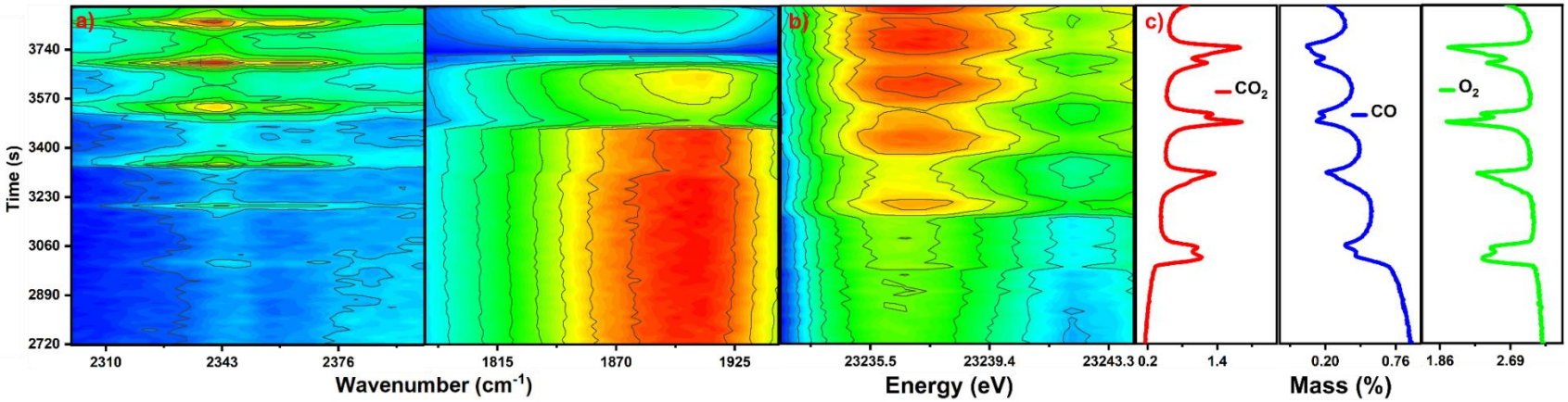

Figure S12 From left to right: a) DRIFTS signature for CO (left) and CO_2 (right) evolution; b) XANES evolution; c) evolution of CO_2, CO, and O_2 concentration as function of time for the position 4.

`

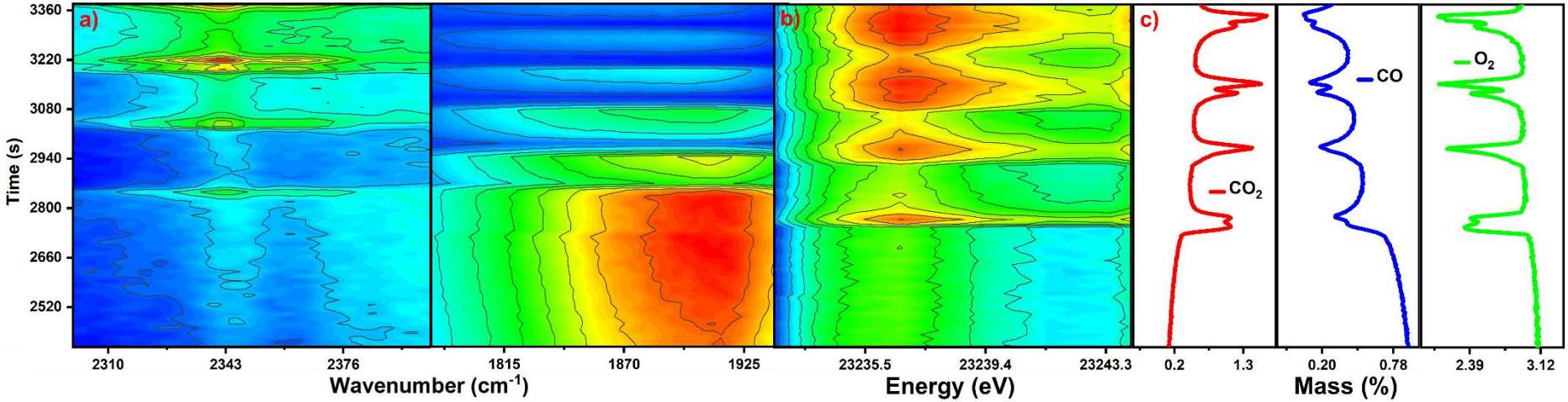

Figure S13 From left to right: a) DRIFTS signature for CO (left) and CO_2 (right) evolution; b) XANES evolution; c) evolution of CO_2, CO, and O_2 concentration as function of time for the position 5.

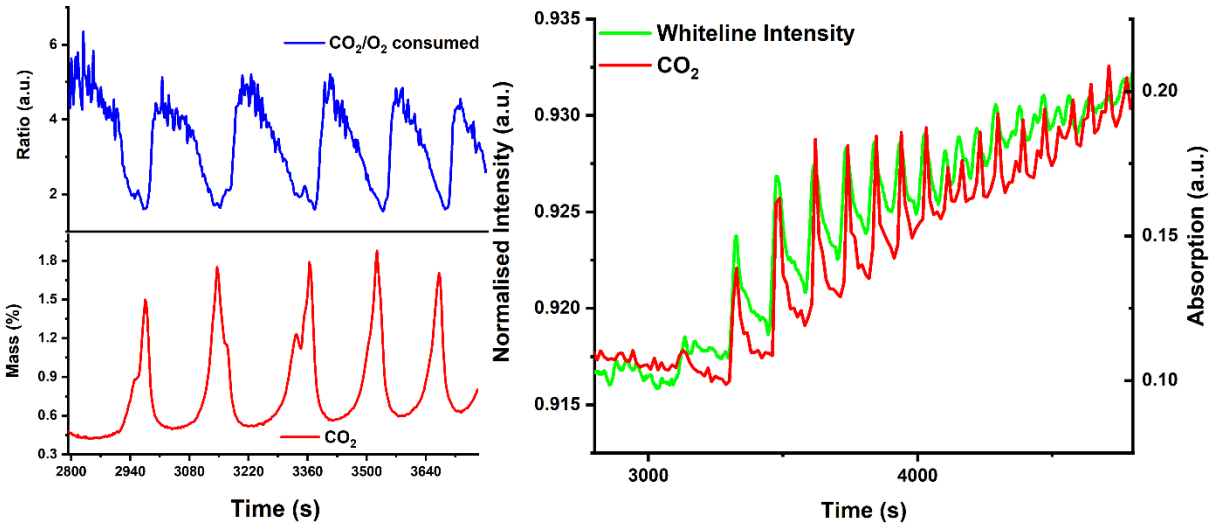

Figure S14. a) CO_2 produced/O_2 consumed (top), CO_2 produced (bottom); b) DRIFTS signal for CO_2(g) and XANES trace as function of time for the position 1 during temperature ramp.

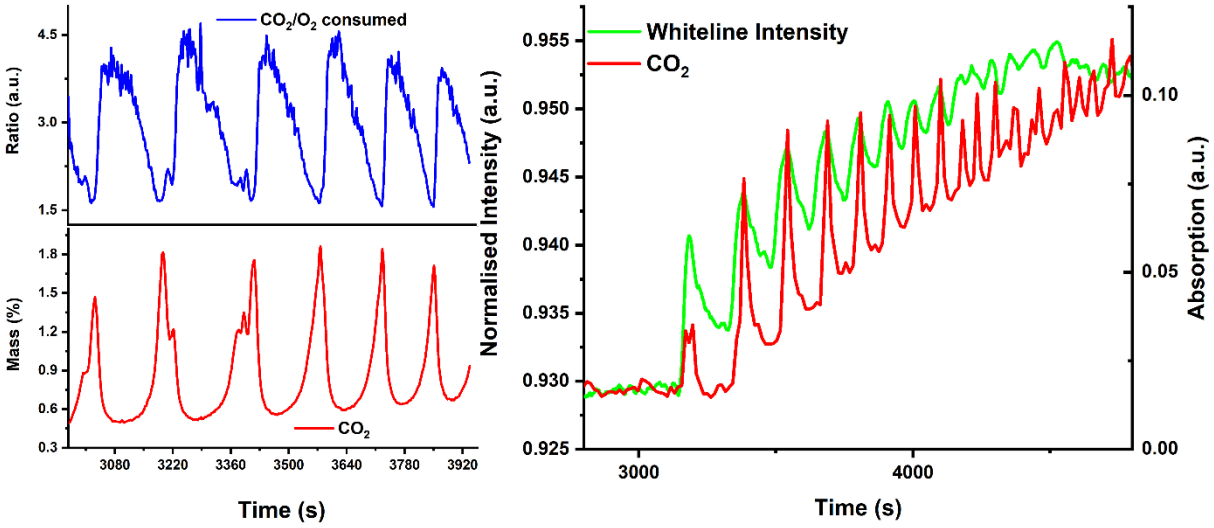

Figure S15. a) CO_2 produced/O_2 consumed (top), CO_2 produced (bottom); b) DRIFTS signal for CO_2(g) and XANES trace as function of time for the position 2 during temperature ramp.

`

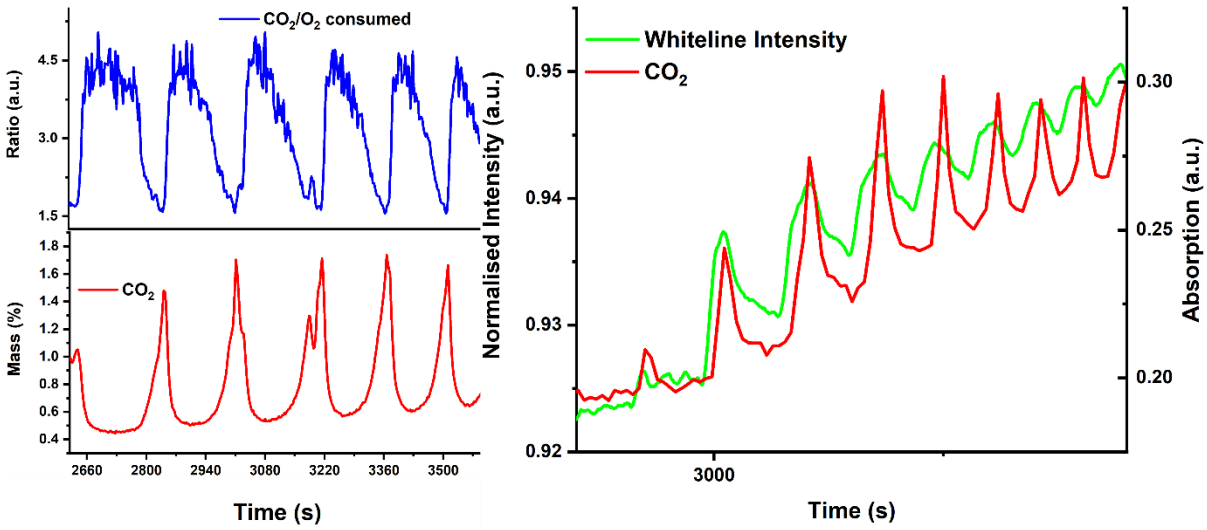

Figure S16. a) CO_2 produced/O_2 consumed (top), CO_2 produced (bottom); b) DRIFTS signal for CO_2(g) and XANES trace as function of time for the position 3 during temperature ramp.

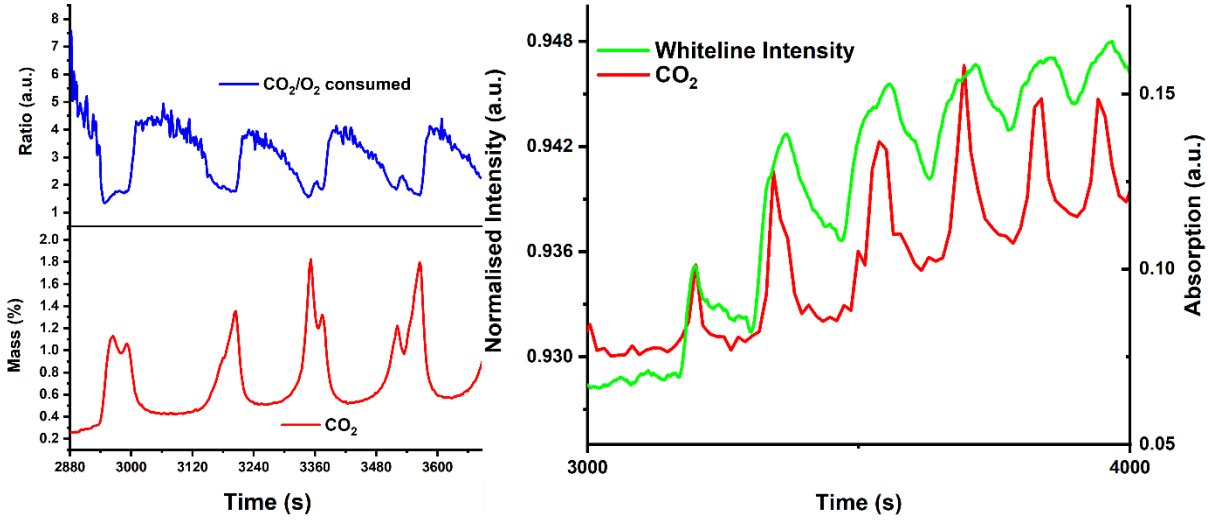

Figure S17. a) CO_2 produced/O_2 consumed (top), CO_2 produced (bottom); b) DRIFTS signal for CO_2(g) and XANES trace as function of time for the position 4 during temperature ramp.

`

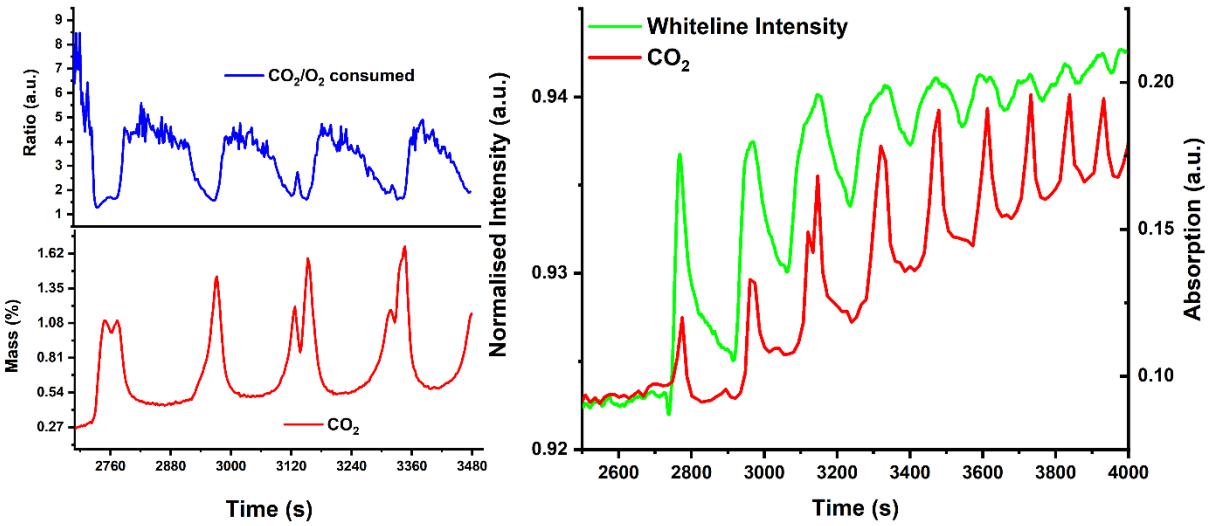

Figure S18. a) CO_2 produced/O_2 consumed (top), CO_2 produced (bottom); b) DRIFTS signal for CO_2(g) and XANES trace as function of time for the position 1 during temperature ramp.

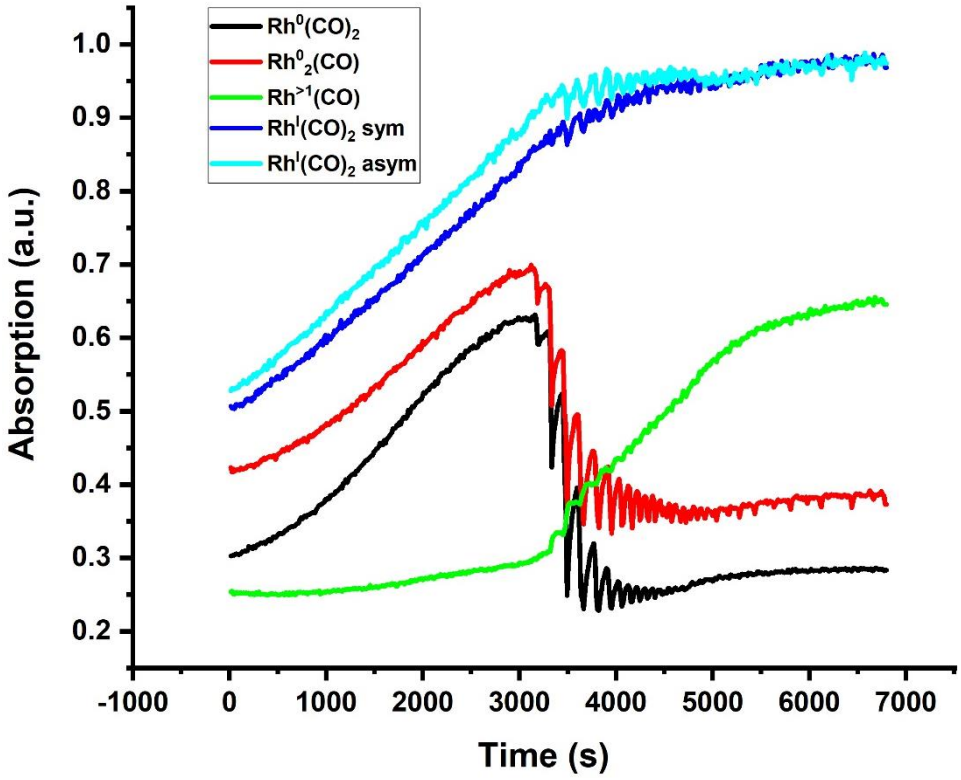

Figure S19: DRIFTS signal for CO adsorbed on Rh at spatial position 6.

X-ray photoelectron spectroscopy (XPS) data

`

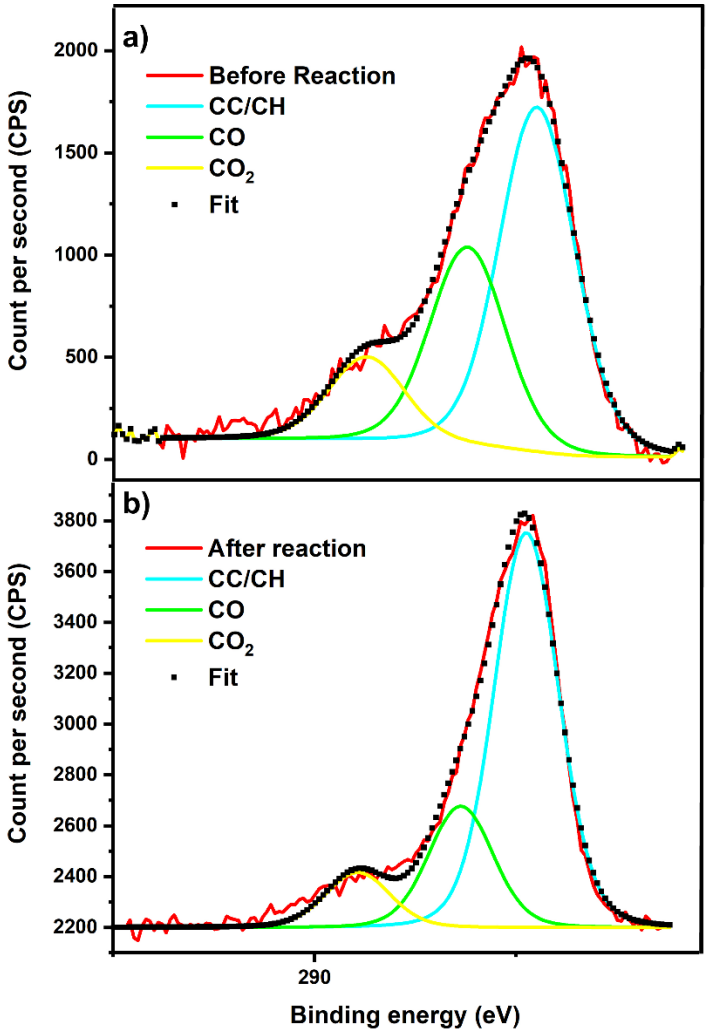

Figure S20. XPS spectra at C energy of Rh/Al_2O_3 before and after reaction.

`

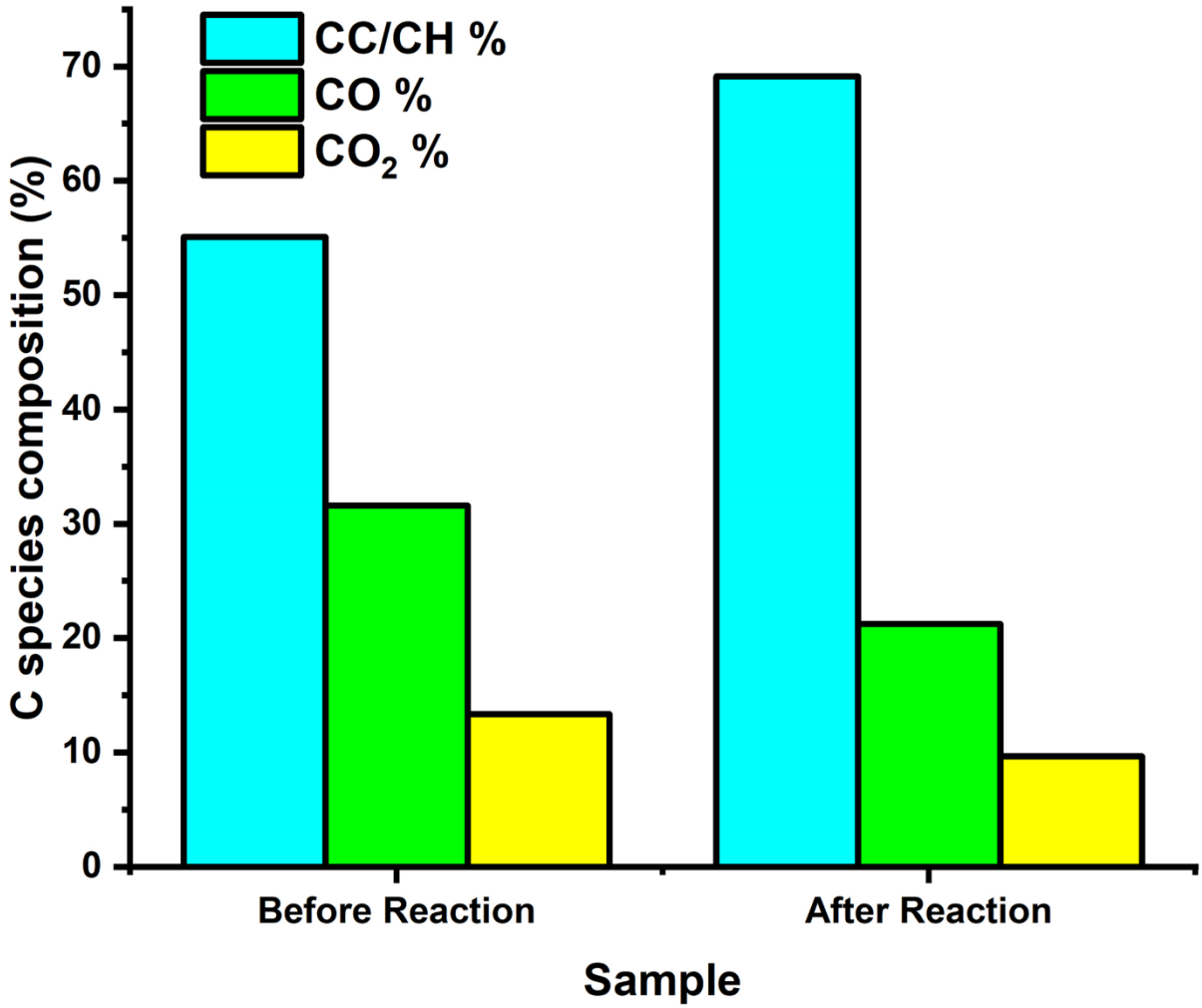

Figure S21. Carbon speciation obtained through XPS of Rh/Al_2O_3 before and after reaction.

`

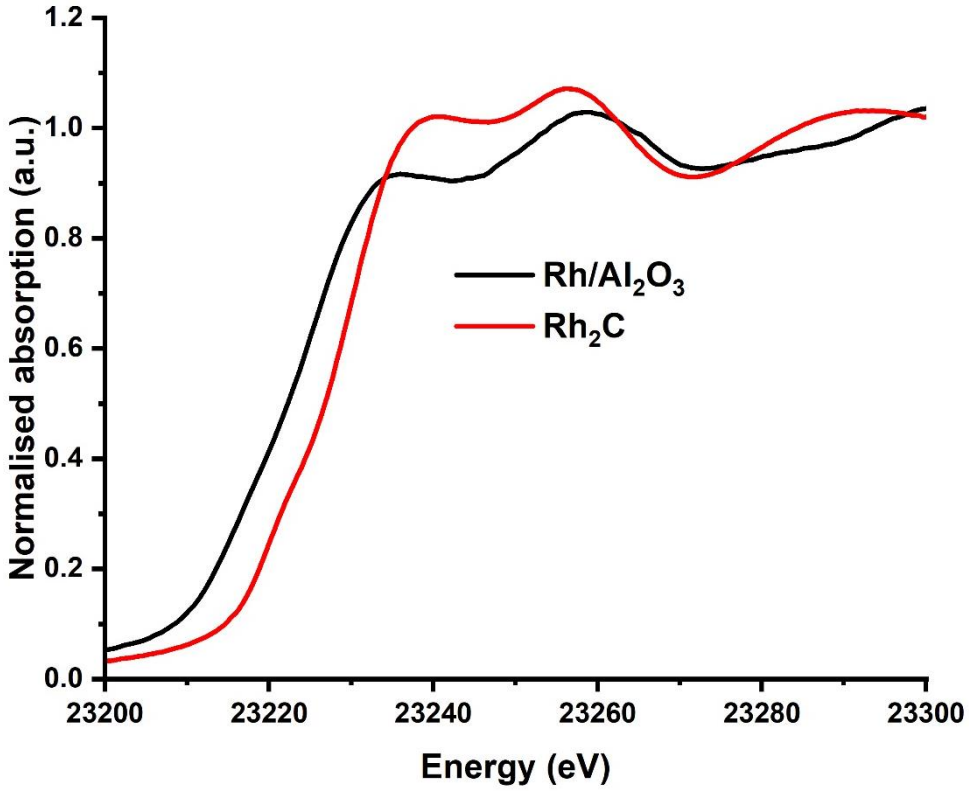

Figure S22. Rh/Al_2O_3 during CO oxidation reaction and Rh_2C XANES data. The data shows a completely different structure in the sample

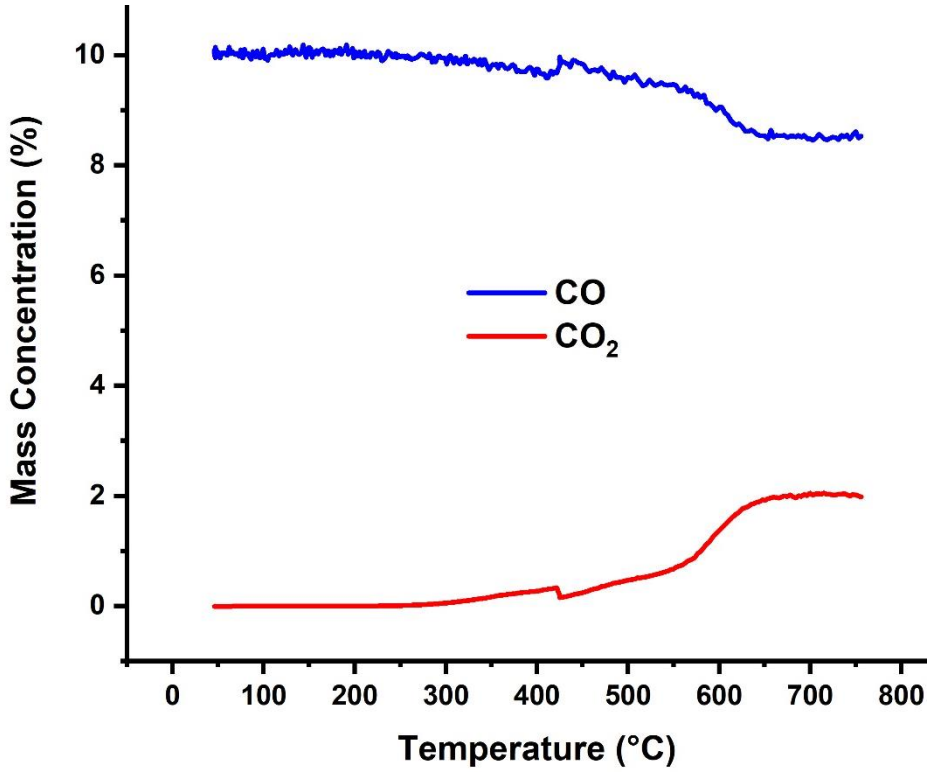

`

Figure S23. Percentage mass concentration for CO and CO_2 (m/z 28 and 44 respectively) obtained through mass spectrometry during CO reaction on Rh/Al_2O_3 in absence of oxygen, as function of temperature.

Computational calculations

The computed $\boldsymbol{\sigma}$ for each surface are reported in Table S1. Consistent with previous studies,(1) our calculated surface energies confirm the {001} surfaces to be the most stable for all the systems investigated.

Table S1. Calculated properties of the (001), (011) and (111) surfaces of Rh. Surface area ($\mathbf{a^2}$) is given in $Å^2$, whilst both unrelaxed ($\boldsymbol{\sigma_{unrel}}$) and relaxed ($\boldsymbol{\sigma_{rel}}$) surface energies are given in J/m^2.

PBE	$\mathbf{a^2}$	$\boldsymbol{\sigma_{unrel}}$	$\boldsymbol{\sigma_{rel}}$
(001)	57.4754	3.85	2.80
(011)	81.2825	3.57	3.23
(111)	99.5504	2.93	2.92
Scan			
(001)	57.4754	3.66	3.64
(011)	79.3530	3.76	3.70
(111)	97.1872	3.40	3.40

Carbon adsorption of carbon was calculated with reference to: bulk graphite, gas phase CO and carbon formed by the oxidation of CO to C + O_2 (see table 1). The values calculated are consistent throughout the two functional benchmarked with the obvious exception of the results with reference to graphite. This is explained by the higher formation energy of the elemental carbon seen using PBE.

`

Table S2. Carbon adsorption. Values shown in eV with reference to: bulk graphite ($\Delta E_{Graphite}$), atomic carbon ($\Delta E_{C,surf}$) or CO – ½ O_2 (ΔE_{CO-O}).

Rh(001)	[a]$\Delta E_{Graphite}$	[a]$\Delta E_{C,Atom}$	[a]ΔE_{CO-O}	[b]$\Delta E_{Graphite}$	[b]$\Delta E_{C,Atom}$	[b]ΔE_{CO-O}
1C	-0.56	-8.60	0.00	-2.30	-8.31	0.00
2C	-0.36	-8.40	0.20	-2.11	-8.13	0.18
3C	-0.27	-8.31	0.29	-1.94	-7.95	0.36
4C	-0.09	-8.13	0.47	-1.69	-7.70	0.61
Rh(011)						
1C	2.04	-6.00	2.59	0.49	-5.53	2.78
2C	0.76	-7.28	1.32	0.49	-5.52	2.79
3C	0.79	-7.25	1.35	0.50	-5.51	2.80
4C	1.12	-6.92	1.67	0.51	-5.50	2.81
Rh(111)						
1C	0.45	-7.59	1.00	-1.24	-7.26	1.05
2C	0.65	-7.39	1.21	-1.21	-7.22	1.09
3C	0.77	-7.27	1.32	-1.15	-7.17	1.14
4C	0.75	-7.29	1.30	-1.03	-7.04	1.27

[a]PBE functional. [b]Scan functional.

Both functional also compute consistent carbon monoxide adsorption energies arose each surface studied with the exception of the values given in reference to the carbonated (011)-surface. This is explained by the low adsorption energy of carbon on this surface as calculated by the PBE functional.

Table S3. Carbon monoxide adsorption. Values shown in eV with reference to either gas phase CO ($\Delta E_{CO,mol}$) or the carbon loaded surface ($\Delta E_{C,surf}$).

Rh(001)	[a]$\Delta E_{CO,mol}$	[a]$\Delta E_{C,surf}$	[b]$\Delta E_{CO,mol}$	[b]$\Delta E_{C,surf}$
1CO	-2.36	-2.36	-2.50	-2.50
2CO	-2.35	-2.55	-2.46	-2.64
3CO	-2.29	-2.58	-2.39	-2.75
4CO	-2.28	-2.75	-2.41	-3.02
Rh(011)				
1CO	-2.28	-3.60	-2.37	-5.16
2CO	-2.29	-3.61	-2.38	-5.17
3CO	-2.28	-3.63	-2.37	-5.16

`

4CO	-2.27	-3.94	-2.36	-5.17
Rh(111)				
1CO	-2.22	-3.22	-2.24	-3.30
2CO	-2.17	-3.38	-2.26	-3.35
3CO	-2.13	-3.46	-2.25	-3.39
4CO	-2.14	-3.44	-2.22	-3.49

[a]PBE functional. [b]Scan functional.

Owing to the consistent performance of both functionals with regards to their predicted adsorption values, it was decided to calculate the reaction mechanisms of each facet with the PBE functional only. Equations S3−5 show the calculated reaction mechanisms depicted in figures 5 (see manuscript), respectively.

$$C + O_2 \rightarrow CO + O \qquad (S3)$$

$$2CO \rightarrow CO_2 + C \qquad (S4)$$

$$CO + O_2 \rightarrow CO_2 + O \qquad (S5)$$

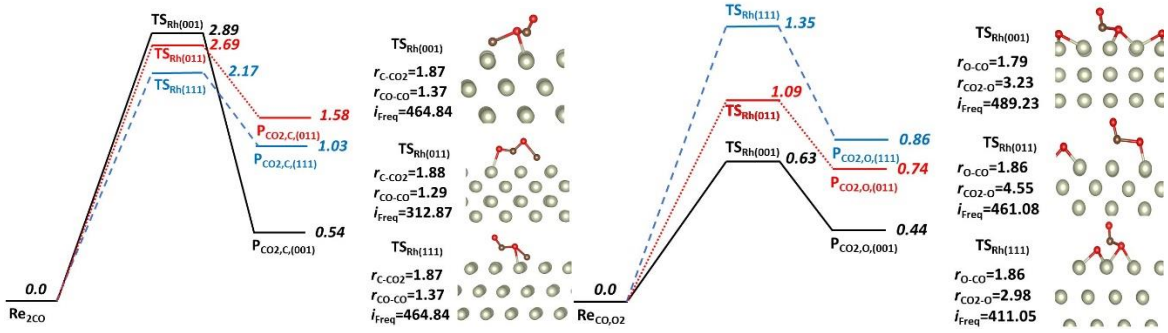

Fig.S24. Reaction landscape surface mediated: (left) Boudouard reaction, (right) carbon oxidation. Reaction landscapes for: (black solid line) Rh(001) surface, (red dotted line) Rh(011) surface and (blue dashed line) Rh(111) surface. All energies are given in eV with important transition state bond distances shown in Å. The negative frequency corresponding to the reaction coordinate for each transition state is given in cm^{-1}.

`

References

1. J. C. W. Swart, P. Van Helden, E. Van Steen, *Journal of Physical Chemistry C*. **111**, 4998–5005 (2007).